crystals

MDPI

Article

Bi_2Te_3/Graphene Heterostructure as the Saturable Absorber for ~1.0 μm Passively Q-switched Solid State Pulsed Laser

Yijian Sun [1] and Houping Xia [2,*]

[1] Faculty of Materials Metallurgy and Chemistry, Jiangxi University of Science and Technology, Ganzhou 341000, China; sunyijian@jxust.edu.cn
[2] College of Physics and Optoelectronics Technology, Baoji University of Arts and Sciences, Baoji 721016, China
* Correspondence: hpxia6688@163.com

Abstract: Due to the tunable nonlinear optical properties of the Bi_2Te_3/graphene heterostructure, stable solid state pulsed lasers based on the Bi_2Te_3/graphene saturable absorber have attracted intensive attention. In this work, the Bi_2Te_3/graphene heterostructure with good nonlinear absorption characteristics was synthesized by a self-assembly solvothermal route, and the optical saturable absorption properties of the saturable absorber were investigated. Owing to the large modulation depth of Bi_2Te_3 nanosheets and the high thermal conductivity of graphene, the Bi_2Te_3/graphene heterostructure saturable absorber shown good nonlinear saturable absorber performance and contributed the improved passively Q-switched Yb^{3+}: $GdAl_3(BO_3)_4$ pulsed laser when compared with that of the pure Bi_2Te_3 based Yb^{3+}: $GdAl_3(BO_3)_4$ laser, no matter pulse width or pulse energy. Our work demonstrates that the Bi_2Te_3/graphene heterostructure was a promising saturable absorber in ~1 μm solid-state pulsed lasers.

Keywords: Bi_2Te_3/graphene; Q-switched laser; Yb^{3+}: $GdAl_3(BO_3)_4$ crystal

check for updates

Citation: Sun, Y.; Xia, H. Bi_2Te_3/Graphene Heterostructure as the Saturable Absorber for ~1.0 μm Passively Q-switched Solid State Pulsed Laser. *Crystals* **2022**, *12*, 222. https://doi.org/10.3390/cryst12020222

Academic Editor: Shujun Zhang

Received: 4 January 2022
Accepted: 29 January 2022
Published: 2 February 2022

Publisher's Note: MDPI stays neutral with regard to jurisdictional claims in published maps and institutional affiliations.

Copyright: © 2022 by the authors. Licensee MDPI, Basel, Switzerland. This article is an open access article distributed under the terms and conditions of the Creative Commons Attribution (CC BY) license (https://creativecommons.org/licenses/by/4.0/).

1. Introduction

For realizing pulsed lasers, an effective method is the passively Q-switching technology because of the compactness and simplicity of the cavity structure. In such a technology, saturable absorber (SA) is the most important component. In the past decades, several kinds of two-dimensional (2D) nanomaterials, including graphene, transition metal dichalcogenides (e.g., MoS_2 and WS_2), topological insulators (TIs, e.g., Bi_2Te_3, Sb_2Te_3, andBi_2Se_3), and black phosphorus, have been used as SAs in both fiber and solid-state Q-switched lasers [1–7]. Among these 2D nanomaterials SAs, graphene is the most popular one due to its broadband absorption, low nonsaturable loss, high damage threshold, and controllable modulation depth [1,8]. Efficient Q-switching fiber and bulk lasers based on graphene SA from the near to middle infrared region have been realized [9–11]. Nevertheless, the pulse energies of these pulsed lasers are prohibited by the relatively low modulation depth of graphene [11]. TIs are another kind of broadband SAs because of the gapless metallic state in their surface states. Compared with graphene SA, Bi_2Te_3 as a typical TI presents much higher modulation depths [12,13], but it is a relatively slower SA with a long relaxation time [14–16]. Furthermore, due to the heavily populated intrinsic defects and low thermal conductivity of Bi_2Te_3, most of the peak powers and pulse energies based on Bi_2Te_3 SAs were also very low [17,18].

Recently, to overcome the shortcomings of graphene SA and Bi_2Te_3 SA when they were used individually, a strategy to controllably grow the Bi_2Te_3/graphene heterostructure with controllable optical properties was provided. The modulation depth of the Bi_2Te_3/graphene heterostructure is much higher than that of monolayer graphene, which benefits from the stronger absorption of Bi_2Te_3 nanocrystals. At the same time, the exciton relaxation time is tunable with the change of Bi_2Te_3 coverage. Using the Bi_2Te_3/graphene heterostructure SA,

Mu et al. realized both Q-switching and mode-locking fiber pulsed lasers at ~1.5 μm [19]. Wang et al. further demonstrated the broadband saturable absorber property and achieved passively mode-locked pulses in both Er^{3+}-doped and Yb^{3+}-doped fiber lasers [20].

Compared with fiber lasers, the solid state lasers were considered to be more liable to obtain high-energy short pulse due to less nonlinear pulse-splitting and larger mode areas [21]. For the solid state pulsed lasers, You et al. investigated ~2 μm and ~3 μm passively Q-switched lasers based on the Bi_2Te_3/graphene heterostructure SA by using the Tm^{3+}: YAP and Er^{3+}: YSGG as the laser gain medium, respectively [22]. Due to the widespread applications in communication, laser detection, and industrial processing, ~1 μm pulsed lasers with high peak power and short pulse duration are still widely concerned. Generally, the Yb^{3+}-doped crystals are promising laser gain material for realizing ~1 μm pulsed lasers because of the simple energy levels, weak electron–phonon coupling, and long upper-state lifetime of Yb^{3+}. To our best knowledge, Bi_2Te_3/graphene SA has not been used to Q-switched Yb^{3+}-doped solid state lasers so far. So, in this work, the Yb^{3+}: $GdAl_3(BO_3)_4$ (Yb^{3+}: GAB) crystal was adopted as the laser gain medium to investigate the high-performance ~1 μm solid state pulsed laser based on the Bi_2Te_3/graphene heterostructure SA.

2. Materials and Methods

There are various strategies to fabricated two-dimensional materials, such as chemical vapor deposition (CVD) [19], vacuum filtration [23], solvothermal method [22], and so on [24–26]. Among them, hydrothermal is a promising method because of its simple preparation process and easiness to achieve large size preparation. So, the Bi_2Te_3/graphene heterostructures in this work were synthesized by a self-assembly solvothermal route [22]. In detail, the used GO was firstly synthesized from graphite powder by the modified Hummers method [27]. Then, all the chemicals used for synthesizing Bi_2Te_3 nanosheets, Na_2TeO_3 (0.1 g), $BiCl_3$ (0.095 g), NaOH (0.12 g), and PVP (0.15 g), were added in graphene oxide (5 mg) which was dissolved in 15 mL ethylene glycol. After ultrasonic stirring for 30 min, the mixed solution was transferred to a 20 mL hydrothermal reactor and then was heated at 180 °C for 36 h. At last, the Bi_2Te_3/graphene heterostructure powder was obtained after cooling, washing, and drying. In this process, the Bi_2Te_3 nucleus could be tightly adsorbed on the GO by oxygen-containing functional groups and grown into Bi_2Te_3 nanosheets. Additionally, the GO could be reduced by ethylene glycol to graphene [22].

The SA was prepared by spin-coating the Bi_2Te_3/graphene heterostructure on quartz substrate. The optical saturable absorption properties of the SA were investigated by open-aperture z-scan technology [22]; here, a homemade ~1.0 μm Q-switched laser source was used.

To obtain the ~1 μm Q-switched laser, a fiber-coupled 976 nm diode laser with a core diameter of 200 μm and a numerical aperture of 0.22 was adopted as the pump source. The laser cavity is a plano-concave cavity with a length of 18 mm. A plane mirror with high-reflection coating at 1020–1080 nm and antireflection coating at 976 nm was used as the input mirror (IM), while the output coupler (OC) was a concave mirror, which has the partial transmission of 3% from 1020 to 1080 nm. The laser gain medium was uncoated 10 at.% Yb^{3+}: GAB crystal with a size of 3 × 3 × 2 mm^3. The Bi_2Te_3/graphene SA was located near the output mirror inside the resonant cavity. The corresponding experimental setup of the passively Q-switched laser is shown in Figure 1.

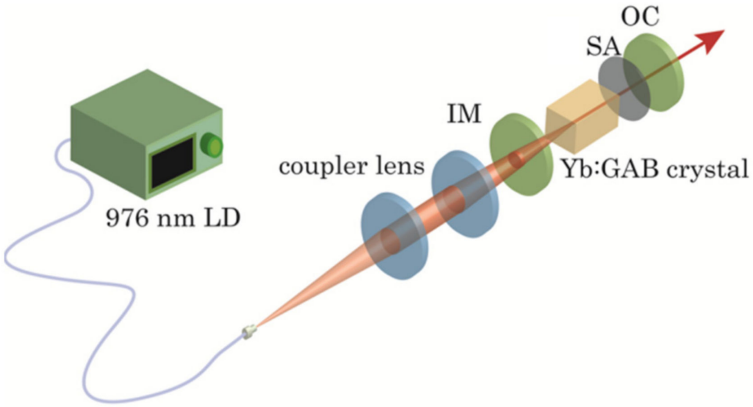


Figure 1. The experimental setup of the passively Q-switched Yb^{3+}: GAB laser.

3. Results and Discussion

Figure 2a shows the XRD patterns of the prepared Bi_2Te_3/graphene heterostructure and the standard diffraction peaks of Bi_2Te_3. It is clear that the diffractions peaks of Bi_2Te_3/graphene heterostructure are in good agreement with those of the hexagonal Bi_2Te_3 phase (JCPDF card No. 15-0863), which indicates the successful synthesis of Bi_2Te_3 nanosheets. However, the typical diffraction peak of graphene cannot be found, which suggests that the existence of Bi_2Te_3 plates inhibited the restacking of graphene sheets [28]. To confirm the presence of graphene, the C1s XPS spectra of Bi_2Te_3/graphene heterostructure and bare Bi_2Te_3 fabricated by the solvothermal method were performed and given in Figure 2b. The peaks of the spectra of Bi_2Te_3/graphene heterostructure correspond to different forms of carbons: non-oxygenated carbon (C–C and C=C, 285 eV), carbonyl carbon (C=O, 288.2 eV). Compared to the strong XPS peaks of C=O and C–O of other works about graphene oxide, the omitted XPS peak of C–O and pretty weak peak of C=O in this work clearly demonstrated the reduction of GO into graphene [28].

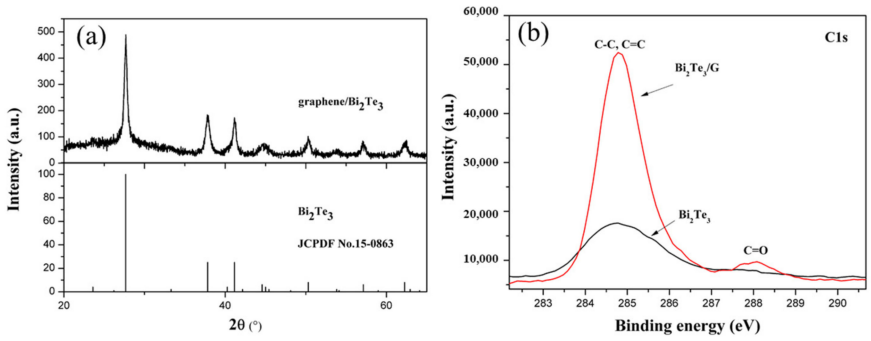


Figure 2. (**a**) XRD of the Bi_2Te_3/graphene heterostructure; (**b**) C1s XPS of the Bi_2Te_3/graphene heterostructure and Bi_2Te_3.

To analyze the morphology and structure of the obtained Bi_2Te_3/graphene sample, the scanning electron microscope (SEM) and the Raman spectra were characterized. Figure 3a displays the SEM image of bare Bi_2Te_3 nanosheets. Obviously, the sample exhibits a hexagonal plate shape. In Figure 3b, the hexagonal Bi_2Te_3 nanosheets absorbed on the graphene surface presents quite sharp edges and a flat surface, which indicates they are well-crystallized. Figure 3c gives the typical Raman spectrum of the Bi_2Te_3 nanosheets, which was excited by a 532 nm laser. Four characteristic peaks at 62, 98, 116, and 140 cm^{-1} are consistent with the vibrational modes of $A_{1g}{}^1$, $E_g{}^2$, $A_{1u}{}^2$, and $A_{1g}{}^2$ for Bi_2Te_3, respectively. Among them, the $A_{1u}{}^2$ peak is used to be the infrared-active mode in bulk crystalline Bi_2Te_3, which becomes Raman-active mode when the bulk breaks into thin films for the symmetry breaking [29,30]. In the Raman spectrum of the Bi_2Te_3/graphene

heterostructure shown in Figure 3d, three vibrational modes of $A_{1g}{}^1$, $E_g{}^2$, and $A_{1u}{}^2$ for Bi_2Te_3 are observed in the low frequency range of 40–180 cm^{-1}. It is worth noting that the vibration strength of $A_{1u}{}^2$ increases as the thickness of Bi_2Te_3 decreases. Consequently, the Bi_2Te_3 nanosheets anchored on the surface of graphene are much thinner than the bare Bi_2Te_3 nanosheets synthesized by the solvothermal route directly, which benefits from the one-sided growth of Bi_2Te_3 on graphene. In the high frequency range of 800–3000 cm^{-1}, there are two Raman peaks of graphene. In detail, the characteristic peak at 1598 cm^{-1} is identified as G band, and another peak at 1330 cm^{-1} can be recognized as D band, which owes to the first-order zone boundary phonons in defective graphene [31].

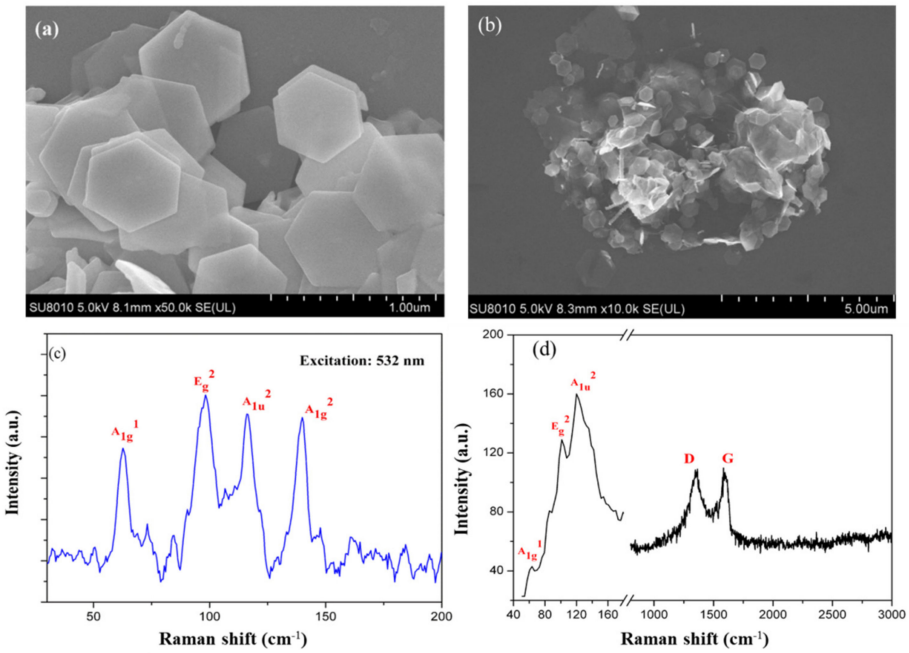


Figure 3. (**a**) SEM image of Bi_2Te_3; (**b**) SEM image of the Bi_2Te_3/graphene heterostructure; (**c**) Raman spectrum of Bi_2Te_3; (**d**) Raman spectrum of the Bi_2Te_3/graphene heterostructure.

The z-scan transmittance depends on the position of Bi_2Te_3/graphene SA shown in Figure 4a. The sharp peak on the curve indicates the good nonlinear absorption characteristics of SA. Furthermore, the relationship between optical transmittances and increased excited intensity can be determined by translating from the z-scan curve, which is given in Figure 4b. In addition, the modulation depth of 26.5%, the saturation intensity of 1.34 MW/cm^2, and the non-saturable losses of 3.1% can be calculated through curve fitting with the formula:

$$T(I) = 1 - \Delta R \times \exp(-I/I_{sat}) - T_{ns} \quad (1)$$

where ΔR, I, I_{sat}, and T_{ns} are the modulation depth, the exciting intensity, the saturation intensity, and the nonsaturable loss, respectively.

Table 1 lists the nonlinear absorption parameters of monolayer graphene SA, Bi_2Te_3 SA, and Bi_2Te_3/graphene SA. It is obvious that the saturation intensity of the bare Bi_2Te_3 nanosheet was pretty low, which can mainly be attributed to the weakened absorption caused by the oxidation of the Bi_2Te_3 nanosheets. When grown on graphene, the surface of the Bi_2Te_3 nanosheet can be protected from oxidation effectively, which is also conducive to improve the modulation depth. Due to the high thermal conductivity of graphene, the nonsaturable loss of Bi_2Te_3/graphene SA was smaller. The relatively lager modulation depth and saturation intensity as well as the lower nonsaturable loss of Bi_2Te_3/graphene SA will be advantageous to the realization of high-performance Q-switched lasers. It is worth noting that the modulation depth and saturation intensity of the Bi_2Te_3/graphene SA in this work are comparable to those of the Bi_2Te_3/graphene SA produced by CVD [32].

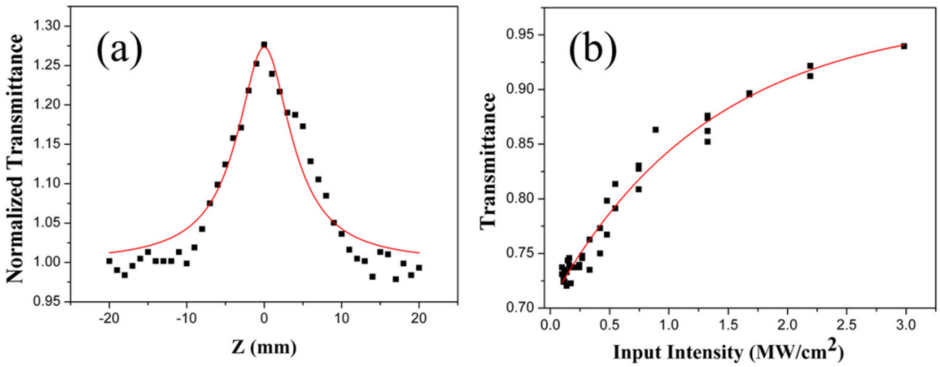


Figure 4. (**a**) Z-scan curve and (**b**) nonlinear saturable absorption curve of Bi_2Te_3/graphene AS.

Table 1. Nonlinear absorption parameters of graphene SA, Bi_2Te_3 SA, and graphene/Bi_2Te_3 SA.

Type of SAs	Modulation Depth	Saturation Intensity	Nonsaturable Loss	Ref.
Monolayer graphene	4.5%	0.8 MW/cm^2	-	
6.5 nm Bi_2Te_3	6.5%	35 W/cm^2	-	[32]
Bi_2Te_3/grapheme(CVD)	23%	0.6 MW/cm^2	-	
Bi_2Te_3	14.29%	16.62 kW/cm^2	4.23%	[33]
Bi_2Te_3/graphene	26.5%	1.34 MW/cm^2	3.1%	This work

A stable passive Q-switching laser operation was realized when the absorbed pump power was increased to be 2.86 W. The output power nearly increased linearly with the absorbed power elevated, and the maximum average output power of 305 mW with a slope efficiency of 11.7% was obtained until the absorbed power was 5.45 W, as shown in Figure 5a. The pulse width and repetition rate depending on the absorbed pump power was presented in Figure 5b. The repetition rate and pulse width varied from 23.6 kHz to 181.1 kHz and 2.65 µs to 280 ns, respectively, in the stable Q-switching regime. Based on the measured repetition rate and average output power, the energy of pulse was estimated and shown in Figure 5a. Obviously, the pulse energy increased monotonically with the pump power up to 4.8 W, with a maximum value of 1.83 μJ. Then, it decreased slightly with the further increased pump power due to the thermal effect in the cavity. Furthermore, the pulse energy was 1.68 μJ under the maximum absorbed power, and the relevant Q-switched laser pulse trains and single pulse are displayed in Figure 6.

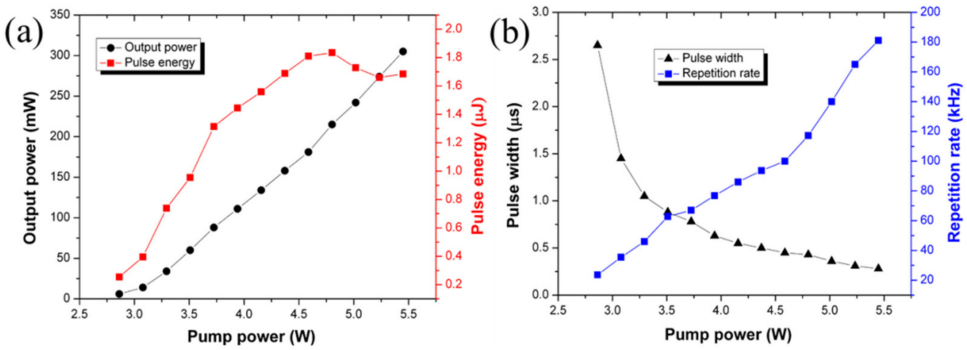


Figure 5. (**a**) The output power and single-pulse energy; (**b**) pulse width and repetition rate over the absorbed pump power.

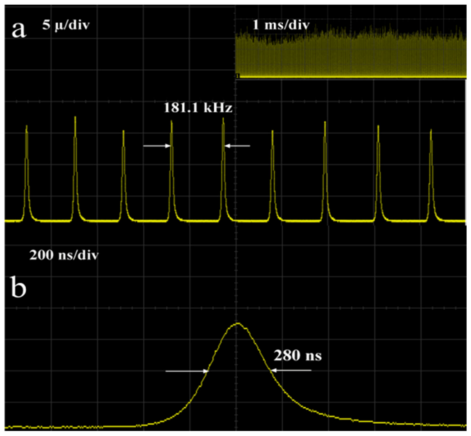


Figure 6. (**a**) The Q-switched pulse trains; (**b**) the single pulse under the absorbed pump power of 5.45 W.

Table 2 shows some excellent ~1 μm passively Q-switched solid state laser performances with 2D SAs. It can be seen that our results are superior to the results yielded by using BP, MoS_2, and Bi_2Te_3. Especially compared with the Q-switched laser performances based on Bi_2Te_3 individually, the shorter pulses and higher power were obtained simultaneously when utilizing the Bi_2Te_3/graphene heterostructure as the SA. Despite the slightly higher output power of Bi_2Se_3 Q-switched Yb: KGW laser, the narrow pulse width in this work will widen the practical application. It is important to note that, besides the SAs, the gain crystals and cavity design strongly influence the Q-switched laser performance. So, it is hopeful that better performance can be realized by coating the crystal or further optimizing the cavity structure.

Table 2. Comparison of ~1 μm passively Q-Switched laser performance using 2D SAs.

Type of SAs	Gain Crystal	Output Power (mw)	Pulse Width (ns)	Repetition Rate (kHz)	Pulse Energy (μJ)	Ref.
Bi_2Te_3	Nd: Lu_2O_3	79	720	94.7	0.83	[18]
BP	Yb: CYA	37	620	113.6	0.33	[31]
MoS_2	Nd: YAP	260	227	232.5	1.11	[34]
Bi_2Se_3	Yb: KGW	439.4	1600	166.7	2.64	[35]
Bi_2Te_3	Yb: CYB	161	416	147.7	1.09	[33]
Bi_2Te_3	Yb: GAB	57	415	111.4	0.51	[36]
Bi_2Te_3/graphene	Yb: GAB	305	280	181.1	1.83	This work

4. Conclusions

In this work, the Bi_2Te_3/graphene heterostructure was successfully fabricated by the solvothermal reaction, and the relevant nonlinear saturable absorption characteristic was also explored. The saturation intensity, modulation depth, and nonsaturable loss were estimated to be 1.34 MW/cm^2, 26.5%, and 3.1%, respectively. By using the Yb^{3+}: GAB crystal as the laser gain medium, the passively Q-switched pulsed laser of ~1 μm was demonstrated. The maximum output power of 305 mW was obtained, corresponding to a pulse width of 280 ns and a repetition rate of 181.1 kHz. The experimental results demonstrate that the Bi_2Te_3/graphene heterostructure is an appropriate SA for Q-switched lasers in near-infrared range.

Author Contributions: Investigation, data curation, Y.S.; writing—review and editing, H.X. All authors have read and agreed to the published version of the manuscript.

Funding: This research was funded by the National Natural Science Foundation of China (grant number 11804007) and Young Talent Fund of University Association for Science and Technology in Shaanxi, China (grant number 20200512).

Data Availability Statement: Not applicable.

Conflicts of Interest: The authors declare no conflict of interest.

References

1. Bao, Q.L.; Zhang, H.; Wang, Y.; Ni, Z.H.; Yan, Y.L.; Shen, Z.X.; Loh, K.P.; Tang, D.Y. Atomic-layer graphene as a saturable absorber for ultrafast pulsed lasers. *Adv. Funct. Mater.* **2009**, *19*, 3077–3083. [CrossRef]
2. Serres, J.M.; Loiko, P.; Mateos, X.; Yumashev, K.; Díaz, F. Tm: $KLu(WO_4)_2$ microchip laser Q-switched by a graphene-based saturable absorber. *Opt. Express* **2015**, *23*, 14108. [CrossRef] [PubMed]
3. Luo, Z.; Huang, Y.; Weng, J.; Cheng, H.; Xu, H. 1.06 μm Q-switched ytterbium-doped fiber laser using few-layer topological insulator Bi_2Se_3 as a saturable absorber. *Opt. Express.* **2013**, *21*, 29516. [CrossRef] [PubMed]
4. Liu, X.Y.; Yang, K.J.; Zhao, S.S.; Li, T.Y.; Qiao, W.C.; Zhang, H.; Zhang, B.T.; He, J.; Bian, J.; Zheng, L.M.; et al. High-power passively Q-switched 2 μm all-solid-state laser based on a Bi_2Te_3 saturable absorber. *Photonics Res.* **2017**, *5*, 461. [CrossRef]
5. Wang, X.H.; Hu, J.Y.; Xu, J.L.; Sun, Y.J.; Xia, H.P.; Tu, C.Y. Sb_2Te_3 as the saturable absorber for the ~2.0 μm passively Q-switched solid state pulsed laser. *RSC Adv.* **2019**, *9*, 29312. [CrossRef]
6. Luan, C.; Zhang, X.; Zhao, J.; Zhao, S.; Yang, K.; Li, T.; Qiao, W.C.; Chu, H.W.; Qiao, J.P.; Wang, J.; et al. High-peak power passively Q-switched 2 μm laser with MoS_2 saturable absorber. *IEEE J. Sel. Top. Quantum Electron.* **2016**, *23*, 66. [CrossRef]
7. Kong, L.C.; Qin, Z.P.; Xie, G.Q.; Guo, Z.N.; Zhang, H. Black phosphorus as broadband saturable absorber for pulsed lasers from 1μm to 2.7 μm wavelength. *Laser Phys. Lett.* **2016**, *13*, 045801. [CrossRef]
8. Nair, R.R.; Blake, P.; Grigorenko, A.N.; Novoselov, K.S.; Booth, T.J.; Stauber, T.; Peres, N.; Geim, A.K. Fine structure constant defnes visual transparency of graphene. *Science* **2008**, *320*, 1308. [CrossRef]
9. Sun, Z.P.; Hasan, T.; Torrisi, F.; Popa, D.; Privitera, G.; Wang, F.Q.; Bonaccorso, F.; Basko, D.M.; Ferrari, A.C. Graphene mode-locked ultrafast laser. *ACS Nano* **2010**, *4*, 803–810. [CrossRef]
10. Wang, Q.; Teng, H.; Zou, Y.W.; Zhang, Z.G.; Li, D.H.; Wang, R.; Gao, C.Q.; Lin, J.J.; Guo, L.W.; Wei, Z.Y. Graphene on SiC as a Q-switcher for a 2 μm laser. *Opt. Lett.* **2012**, *37*, 395–397. [CrossRef]
11. Martinez, A.; Sun, Z. Nanotube and graphene saturable absorbers for fiber lasers. *Nat. Photon.* **2013**, *7*, 842–845. [CrossRef]
12. Chen, S.Q.; Zhao, C.J.; Li, Y.; Huang, H.H.; Lu, S.B.; Zhang, H.; Wen, S.C. Broadband optical and microwave nonlinear response in topological insulator. *Opt. Mater. Express.* **2014**, *4*, 587–596. [CrossRef]
13. Lu, S.B.; Zhao, C.J.; Zou, Y.H.; Chen, S.Q.; Chen, Y.; Li, Y.; Zhang, H.; Wen, S.C.; Tang, D.Y. Third order nonlinear optical property of Bi_2Se_3. *Opt. Express.* **2013**, *21*, 2072–2082. [CrossRef] [PubMed]
14. Hajlaoui, M.; Papalazarou, E.; Mauchain, J.; Lantz, G.; Moisan, N.; Boschettoet, D.; Jiang, Z.; Miotkowski, I.; Chen, Y.P.; Taleb-Ibrahimi, A.; et al. Ultrafast surface carrier dynamics in the topological insulator Bi_2Te_3. *Nano Lett.* **2012**, *12*, 3532–3536. [CrossRef]
15. Wang, Y.H.; Hsieh, D.; Sie, E.J.; Steinberg, H.; Gardner, D.R.; Lee, Y.S.; Jarillo-Herrero, P.; Gedik, N. Measurement of intrinsic Dirac fermion cooling on the surface of the topological insulator Bi_2Se_3 using timeresolved and angle-resolved photoemission spectroscopy. *Phys. Rev. Lett.* **2012**, *109*, 127401. [CrossRef]
16. Glinka, Y.D.; Babakiray, S.; Johnson, T.A.; Bristow, A.D. Ultrafast carrier dynamics in thin-films of the topological insulator Bi_2Se_3. *Appl. Phys. Lett.* **2013**, *103*, 151903. [CrossRef]
17. Xu, J.L.; Sun, Y.J.; He, J.L.; Wang, Y.; Zhu, Z.J.; You, Z.Y.; Li, J.F.; Chou, M.M.C.; Lee, C.K.; Tu, C.Y. Ultrasensitive nonlinear absorption response of large-size topological insulator and application in low-threshold bulk pulsed lasers. *Sci. Rep.* **2015**, *5*, 14856. [CrossRef]
18. Wang, B.L.; Yu, H.H.; Zhang, H.; Zhao, C.J.; Wen, S.C.; Zhang, H.J.; Wang, J.Y. Topological insulator simultaneously Q-switched dual-wavelength Nd:Lu_2O_3 laser. *IEEE Photon. J.* **2014**, *6*, 1501007. [CrossRef]
19. Mu, H.R.; Wang, Z.T.; Yuan, J.; Xiao, S.; Chen, C.Y.; Chen, Y.; Song, J.C.; Wang, Y.S.; Xue, Y.Z.; Zhang, H.; et al. Graphene–Bi_2Te_3 heterostructure as saturable absorber for short pulse generation. *ACS Photonics* **2015**, *2*, 832–841. [CrossRef]
20. Wang, Z.T.; Mu, H.R.; Yuan, J.; Zhao, C.J.; Bao, Q.L.; Zhang, H. Graphene-Bi_2Te_3 heterostructure as broadband saturable absorber for ultra-short pulse generation in Er-doped and Yb-doped fiber lasers. *IEEE J. Sel. Top. Quantum Electron.* **2016**, *23*, 195–199. [CrossRef]
21. Yu, H.H.; Zhang, H.; Wang, Y.C.; Zhao, C.J.; Wang, B.L.; Wen, S.C.; Zhang, H.J.; Wang, J.Y. Topological insulator as an optical modulator for pulsed solid-state lasers. *Laser Photon. Rev.* **2013**, *7*, L77–L83. [CrossRef]
22. You, Z.Y.; Sun, Y.J.; Sun, D.L.; Zhu, Z.J.; Wang, Y.; Li, J.F.; Tu, C.Y.; Xu, J.L. High performance of a passively Q-switched mid-infrared laser with Bi_2Te_3/graphene composite SA. *Opt. Lett.* **2017**, *42*, 871–874. [CrossRef] [PubMed]
23. Gao, T.; Huangn, K.; Qi, X.; Li, H.X.; Yang, L.W.; Zhong, J.X. Free-standing SnO2 nanoparticles@graphene hybrid paper for advanced lithium-ion batteries. *Ceram. Int.* **2014**, *40*, 6891–6897. [CrossRef]
24. Maleki-Ghaleh, H.; Siadati, M.H.; Fallah, A.; Koc, B.; Kavanlouei, M.; Khademi-Azandehi, P.; Moradpur-Tari, E.; Omidi, Y.; Barar, J.; Beygi-Khosrowshahi, Y.; et al. Antibacterial and Cellular Behaviors of Novel Zinc-Doped Hydroxyapatite/Graphene Nanocomposite for Bone Tissue Engineering. *Int. J. Mol. Sci.* **2021**, *22*, 9564. [CrossRef]
25. Luo, T.; Chen, X.C.; Wang, L.; Wang, P.; Li, C.C.; Iqbal, S.; Cao, B.Q. Ultrafast synthesis of SiC@graphene nanocomposites by one-step laser induced fragmentation and decomposition. *Ceram. Int.* **2018**, *44*, 19028–19032. [CrossRef]

26. Dargahi, Z.; Asgharzadeh, H.; Maleki-Ghaleh, H. Synthesis of Mo-doped TiO2/reduced graphene oxide nanocomposite for photoelectrocatalytic applications. *Ceram. Int.* **2018**, *44*, 13015–13023. [CrossRef]
27. Ju, H.; Kim, M.; Kim, J. A facile fabrication of n-type Bi_2Te_3 nanowire/graphene layer-by-layer hybrid structures and their improved thermoelectric performance. *Chem. Eng. J.* **2015**, *275*, 102–112. [CrossRef]
28. Tu, F.F.; Xie, J.; Cao, G.S.; Zhao, X.B. Self-assembly of Bi_2Te_3-nanoplate/Graphene-nanosheet hybrid by one-pot route and its improved Li-storage properties. *Materials* **2012**, *5*, 1275–1284. [CrossRef]
29. Shahil, K.M.F.; Hossain, M.Z.; Teweldebrhan, D.; Balandin, A.A. Crystal symmetry breaking in few-quintuple Bi_2Te_3 films: Applications in nanometrology of topological insulators. *Appl. Phys. Lett.* **2010**, *96*, 153103. [CrossRef]
30. Zhao, Y.M.; Zhao, Y.; Hughes, R.W.; Su, Z.; Zhou, W.; Gregory, D.H. One-step synthesis of bismuth telluride nanosheets of a few quintuple layers in thickness. *Angew. Chem. Int. Ed.* **2011**, *50*, 10397–10401. [CrossRef]
31. Ma, J.; Lu, S.B.; Guo, Z.N.; Xu, X.D.; Zhang, H.; Tang, D.Y.; Fan, D.Y. Few-layer black phosphorus based saturable absorber mirror for pulsed solid-state lasers. *Opt. Exp.* **2015**, *23*, 22643–22648. [CrossRef] [PubMed]
32. Lan, J.C.; Qiao, J.; Sung, W.H.; Chen, C.H.; Jhang, R.H.; Lin, S.H.; Ng, L.R.; Liang, G.; Wu, M.Y.; Tu, L.W. Role of carrier-transfer in the optical nonlinearity of graphene/Bi_2Te_3 heterojunctions. *Nanoscale* **2020**, *12*, 16956–16966. [CrossRef]
33. Sun, Y.J.; Lee, C.K.; Wang, Y.; Xia, H.P.; Wang, X.H.; You, Z.Y.; Tu, C.Y.; Xu, J.L. Passively Q-Switched Wavelength-Tunable Bulk Laser Using Topological Insulator at 1 μm. *IEEE Photon. Technol. Lett.* **2016**, *28*, 2764–2767. [CrossRef]
34. Lou, F.; Zhao, L.W.; He, J.L.; Jia, Z.T.; Su, X.C. Nanosecond-pulsed, dual-wavelength, passively Q-switched ytterbium-doped bulk laser based on few-layer MoS_2 saturable absorber. *Photon. Res.* **2015**, *3*, A25–A29. [CrossRef]
35. Hu, M.T.; Lin, J.H.; Tian, J.R.; Dou, Z.Y.; Song, Y.R. Generation of Q-switched pulse by Bi_2Se_3 topological insulator in Yb: KGW laser. *Laser Phys. Lett.* **2014**, *11*, 115806. [CrossRef]
36. Sun, Y.J.; Lee, C.K.; Xu, J.L.; Zhu, Z.J.; Wang, Y.Q.; Gao, S.F.; Xia, H.P.; You, Z.Y.; Tu, C.Y. Passively Q-switched tri-wavelength Yb^{3+}:$GdAl_3(BO_3)_4$ solid-state laser with topological insulator Bi_2Te_3 as saturable absorber. *Photon. Res.* **2015**, *3*, A97–A101. [CrossRef]